Lasers in Manufacturing Conference 2019

Micro Laser Lap Welding of Thin SS304 Sheet

S. Patel[a], A. Aggrawal[a], A. Kumar[a*], V.K. Jain[b]

[a]*Department of Mechanical Engineering, Indian Institute of Technology Kanpur, Kanpur - 208016, India*
[b]*At present: Mechanical Engineering Department, Maulana Azad National Institute of Technology, Bhopal- 462003, India*

Abstract

Laser micro welding involves very small melt pool, and rapid cooling and solidification of molten metal. In this study, lap joint experiments of 100 µm SS304 thin sheet were carried out using a continuous wave fiber laser. The set of process parameters leads to acceptable lap joint is identified. Scanning electron and optical microscopy, micro hardness and tensile shear tests of the welded lap joints were carried out to examine the metallurgical and mechanical properties. Thereafter, a 3D computational model has been developed to understanding the process physics and the influence of various process parameters on the weld bead profile quantitatively. The phenomenon of heat transfer, fluid flow, melting, solidification and evaporation are incorporated into the model. The model is used to describe the free surface thermo-fluid behavior, melt pool characteristics and the solidification characteristics. The simulated results of melt pool are in good agreement with the experimental measurement.

Keywords: Micro Laser Welding; Lap Joint, Stainless Steel; Modelling and Simulation.

1. Introduction

Laser welding is a widely used in many manufacturing industry, due to its advantage such as high welding speed, high accuracy, low heat input, non-contact mode, low cost, etc. however welding of micro parts creates many problem due to scaling effect. The lap joint of laser welding is not symmetric about plane or axis, therefore it suffer variable mechanical as well as metallurgical properties from point to point resulting in residual stress, surface cracks, notch effect, porosity formation, etc. Hence optimum selection and control of welding process parameter is required for better lap joint [1].

* Corresponding author. Tel.: +91-512-259-7484; fax: +91-512-259-7408.
E-mail address: arvindkr@iitk.ac.in.

Only few number of researcher in this area were carried out the work for in-depth understanding and reduce the defects in the welded zone. W. Meng et al. (2019) used two high speed cameras to capture the real time images of molten pool and plume for analyzing the static and dynamic behavior of molten metal. It is found that the static and dynamic behavior is mainly depend on the molten pool length, plume area and peak frequency [2]. S. Zhou et al. (2011) found that the dual beam laser welding of lap joint shows spatter free as well as smooth appearance of weld surface with better mechanical properties of high strength galvanized steel [3]. S. E. Manuela et al. (2014) experimentally analysed the effect of process parameter on microstructure and geometry of the weld bead of laser welding of lap joint of austenitic stainless steel. It is also found that tensile strength of weld joint is similar to the base metal [4]. J. ning et al. (2019) investigated that the porosity formation in weld bead is the main cause of mechanical properties reduction for laser welded lap joints of TZM alloy. It is also evident that specimen fails with river pattern during the tensile-shear test of lap welded joint [5]. L. Pellone et al. (2019) studied the porosity formation and mechanical properties by analyzing the longitudinal and perpendicular sections of the laser welded lap joints of aluminium alloy AA6061. It is also found that the reduction of porosity, improvement of mechanical properties and weld seam quality can achieve by using shielding gas [6]. S.K. Cho et al. (2004) investigate the fatigue behavior of laser welded lap joint of SPCC steel. The fatigue strength of longitudinally weld joint was lower than transverse weld joint [7]. Y. Miyazaki and S. Furusako (2007) investigated that the fracture occurs at the weld metal, portion adjacent to the weld joint and base metal for different laser process parameter during tensile shear test [8]. C. Seang et al. (2013) investigate the hardness of laser welded lap joint of DP600 steel by numerical and experimental approach. The hardness was higher in fusion and heat effected zone due to the formation of martensite [9]. S. Patel et al. (2018) developed the numerical modal and validate experimentally for conduction mode laser micro welding. It is found that the maximum velocity and maximum temperature depends on the laser scanning speed linearly [10].

In this paper, a combined experimental and numerical study of laser welding of lap joint is studied. Firstly, a set of experimental study was performed to understand the various implication of this process. Where, further tests were performed to examine the inherent physical properties of laser welded lap joint. Subsequently, a compact three-dimensional numerical model was developed for the comprehensive study of process parameters involved. Where, further quantitative analysis with respect to corresponding experiment were performed to reinforce our understanding of thermal and flow behavior of melt pool during laser welding of lap joint.

2. Experimental Procedure

The experiments were perform using 100 W continuous Yb:YAG fiber laser on 100 µm SS304 thin sheet. The laser beam of 1070 nm wavelength was focused with 50 µm on top surface of the specimens using f-θ lens. The scanning speed of laser was achieved by Galvano scanner. The shielding of argon gas was used for the protective atmosphere during the laser welding of lap joint. The parameter used in experiment is given in table 1.

Table 1. Process parameters used in experiments

Parameter	**Value**
Laser spot diameter (µm)	50
Laser power (W)	100
SS304 sheet thickness (µm)	100
Scanning speed (mm s^{-1})	100, 200, 300, 400, 500

3. Model Description

A three- dimensional finite volume transient heat transfer and fluid flow model is developed to study the transport phenomena in the laser welding of lap joint. The model was implemented using open source C++ code OpenFOAM. The Fig.1 shows the schematic and dimensions of the computational domain. The thermophysical properties of SS304 used in simulation is given in Table 2.

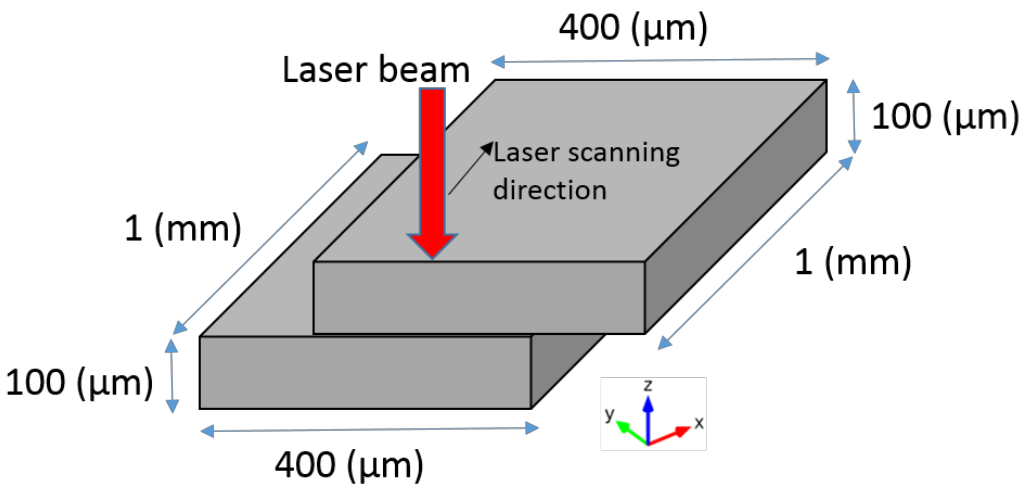

Fig. 1. Schematic of computational domain

The following assumptions were made in the simulation:

- Incompressible and laminar flow was considered in the melt pool.
- The thermophysical properties of SS304 are considered as constant with different values for solid and liquid phases.

Table 2. Thermophysical properties of 304 Stainless steel

Liquidus Temperature (K)	1727
Solidus Temperature (K)	1697
Solid specific heat (J kg^{-1} K^{-1})	711.8
Liquid specific heat (J kg^{-1} K^{-1})	837.4
Solid Thermal conductivity (W m^{-1} K^{-1})	19.63
Liquid Thermal conductivity (W m^{-1} K^{-1})	167.5
Density (kg m^{-3})	7200
Latent heat of fusion (kJ K^{-1})	246
Dynamic viscosity (N m^{-1} s^{-1})	0.06
Thermal expansion coefficient (K^{-1})	1.96×10^{-5}
Surface tension coefficient (N m^{-1} K^{-1})	-0.43×10^{-3}
Absorptivity	0.27

3.1. Governing Transport Equations

The free surface dynamics is captured by VOF method, which is given by

$$\frac{\partial F}{\partial t}+\nabla\cdot\left(\vec{u}F\right)-F\nabla\cdot\vec{u}=0 \qquad (1)$$

where *F* is the volume fraction of phase($0 \le F \le 1$), $\vec{u}$ *is* flow velocity and *t* is time. For the full metal occupied cell $F = 1$ and for full air occupied cell $F = 0$.

The continuity equation is given by

$$\nabla\left(\vec{u}\right)=0 \qquad (2)$$

where $\vec{u}$ is the velocity vector

The energy conservation equation is given by

$$\frac{\partial(\rho C_P T)}{\partial t}+\vec{u}\nabla\left(\rho C_p T\right)=\nabla\left(K\nabla T\right)-\rho L\frac{\partial f_l}{\partial t}+qlaser-qloss \qquad (3)$$

where *K* denotes the thermal conductivity, C_p denotes the heat capacity of the material, ρ denotes the density, *L* denotes latent heat and f_l liquid fraction.

The source term qlaser is the moving laser heat input given by

$$qlaser=\frac{2\eta P}{\pi {R_o}^2}e^{\left(-2\left((x-Vt)^2+(y)^2\right)/R_o^2\right)}\times\left|\nabla F\right|\times\left[\frac{2\rho C_{p\ eff}}{\rho_{metal}C_{p\ metal}+\rho_{gas}C_{p\ gas}}\right] \qquad (4)$$

where η is the absorptivity, *P* is the power of laser beam, *V* is the laser scanning speed, *t* is the time and R_o is the laser spot radius.

The source term qloss involved the heat losses due to radiation, convection and vaporization, which is given by

$$qloss=\left(\varepsilon\sigma_b\left(T^4-T_a^4\right)+h\left(T-T_a\right)+L_v M\right)\times\left|\nabla F\right|\times\left[\frac{2\rho C_{p\ eff}}{\rho_{metal}C_{p\ metal}+\rho_{gas}C_{p\ gas}}\right] \qquad (5)$$

where the value of convective heat transfer coefficient h =10, the value of emissivity ε = 0.45, σ_b is the Stefan-Boltzmann constant ,T_a is ambient temperature, L_v is the latent heat of vaporization and M is the mass flow rate.

The momentum conservation equation is given by

$$\frac{\partial\left(\rho\vec{u}\right)}{\partial t}+\vec{u}\nabla\left(\rho\vec{u}\right)=-\nabla p+\nabla(\mu\left(\nabla\vec{u}+\left(\nabla\vec{u}\right)^{T}\right)+\overrightarrow{F_{damp}}+\overrightarrow{F_{N}}+\overrightarrow{F_{T}}+\overrightarrow{P_{r}} \quad (6)$$

The source term $\overrightarrow{F_{damp}}$ is the damping factor associated with mushy region, which is described by the Carman-Kozeny equation given by

$$\overrightarrow{F_{damp}}=\frac{\left(1-f_{l}\right)^{2}}{f_{l}^{3}+c}K_{c}\vec{u} \quad (7)$$

where the value of permeability coefficient K_c is considered 100,000 kg m^{-3} s^{-1}. The term c is a constant with very small value to avoid division by zero. Liquid fraction f_l is defined as

$$f_{l}=\begin{pmatrix}0 & T<T_{solidus}\\ \frac{T-T_{solidus}}{T_{liquidus}-T_{solidus}} & T_{solidus}\le T<T_{liquidus}\\ 1 & T\ge T_{liquidus}\end{pmatrix} \quad (8)$$

where $T_{solidus}$ and $T_{liquidus}$ represent solidus and liquidus temperature, respectively.

The source term $\overrightarrow{F_N}$ represent the natural convection, which is described by Boussinesq approximation given by

$$\overrightarrow{F_{N}}=\rho_{liq}\vec{g}\beta\left(T-T_{ref}\right) \quad (9)$$

where ρliq , β and Tref represents the density of liquid, coefficient of thermal expansion and reference temperature, respectively.

The source term $\overrightarrow{F_T}$ represents the Marangoni force, which is acting on the liquid- gas interface given by

$$\overrightarrow{F_{T}}=\left(\sigma k\hat{n}+\frac{d\sigma}{dT}\left[\nabla T-\hat{n}\left(\hat{n}\cdot\nabla T\right)\right]\right)\times\left|\nabla F\right|\times\left[\frac{2\rho}{\rho_{metal}+\rho_{gas}}\right] \quad (10)$$

where σ is the surface tension coefficient, κ is curvature of the free surface, $\hat{n}$ is the unit normal vector.

The source term $\overrightarrow{P_r}$ represents recoil vapor pressure given by

$$\overrightarrow{P_r} = \left(0.54 P_0 \exp\left[\frac{L_v M \left(T - T_v \right)}{R T T_v} \right] \right) \hat{n} \times \left| \nabla F \right| \times \left[\frac{2\rho}{\rho_{metal} + \rho_{gas}} \right] \quad (11)$$

where P_0 is the ambient pressure, T_v is the evaporation temperature, R is the universal gas constant.

3.2. Numerical Implementation

The numerical model for the simulation of laser based lap joint welding was developed in OpenFOAM. For this purpose the VOF based interFOAM solver for fluid flow simulation was modified to accommodate heat transfer along with phase change. The VOF equation in OpenFOAM is iteratively solved using the multi-dimensional universal limiter with the explicit solution (MULES) method.

In this study a uniform mesh distribution of 150000 elements was found to be grid independent with a unit mesh size of 10 µm ×10 µm ×10 µm. A varying time step size restricted by Courant-Friedrichs-Lewy (CFL) criteria was used in this simulation for ensuring the stability of solver with regards to time step size.

4. Result and Discussion

4.1. Experimental results

After the laser micro welding of lap joint, the samples were prepared for Scanning electron and optical microscopy using polishing technique and etched in Aqua regia for 10s very carefully. Figure. 2(a) shows the cross-sectional view of welded joint. From figure, it is clearly observed that the melt pool shape is deeper and narrow and penetrate in to both plates, which confirms the keyhole mode laser welding of lap joint. Fig. 2(b) shows the shining top view of weld joint, which also conform the defect free good laser welded lap joint.

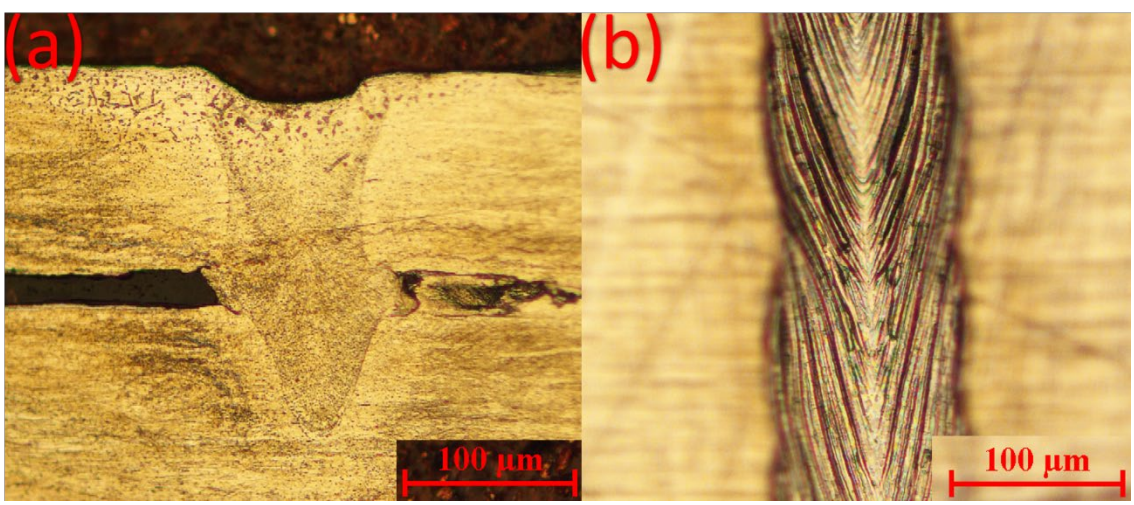

Fig. 2. Experimental result of melt pool for P = 100 W and 300 mm/s scanning seed (a) cross section (b) top view

The tensile shear test specimens were prepare according to ASTM E8. The test was performed on Instron-1195 universal testing machine with a constant displacement rate of 0.1 mm/min. The normal tensile specimen of base metal was also prepared to compare with welded shear tensile test. Fig. 3(a) shows the behavior of maximum load with respect to welding speed. The welded sample of 300 mm/s shows the maximum load among all welded sample, which conforms the welding at 300 mm/s with the power 100W and spot diameter 50 µm gives optimum weld quality of lap joint. The welded sample with scanning speed 300 mm/s provides the 54.53% load to the base metal, which also conforms the good weld joint. Fig. 3(b) shows the maximum elongating at different welding speed.

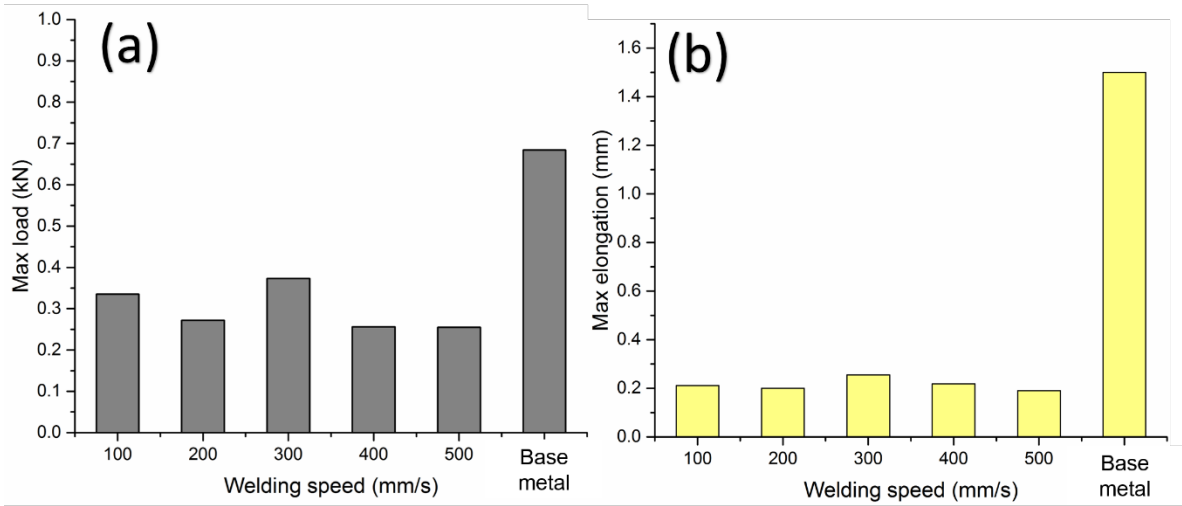

Fig. 3. Comparison of Variation of (a) maximum load, (b) maximum elongation with the laser scanning speed.

The micro hardness test also performed along the weld width using Bareiss D-89610 testing machine with 100gm load and 10 sec dwell time. The result shows the significant drop in hardness in melt pool (223±10 HV) as compare to interface (301±15) and base metal (415±10). Which is due to the removal of strain hardening during the manufacturing of thin sheet by rolling process.

4.2. Model Validation

The melt pool geometry obtained from developed transient numerical model of laser welded lap joint is compared with an in-house experimental geometry. Fig. 4 shows the compression of cross sectional view of both computed melt pool geometry and experimental melt pool geometry. The melt pool geometry of developed model is taken at 1.8 ms of 300 mm/s laser scanning speed at 100 W power and 50 µm diameter. In Fig. 4 melt pool depth and width of numerically computed result are in good agreement with experimental result. The maximum deviation of width is 16.2 % and depth is 7.12 %.

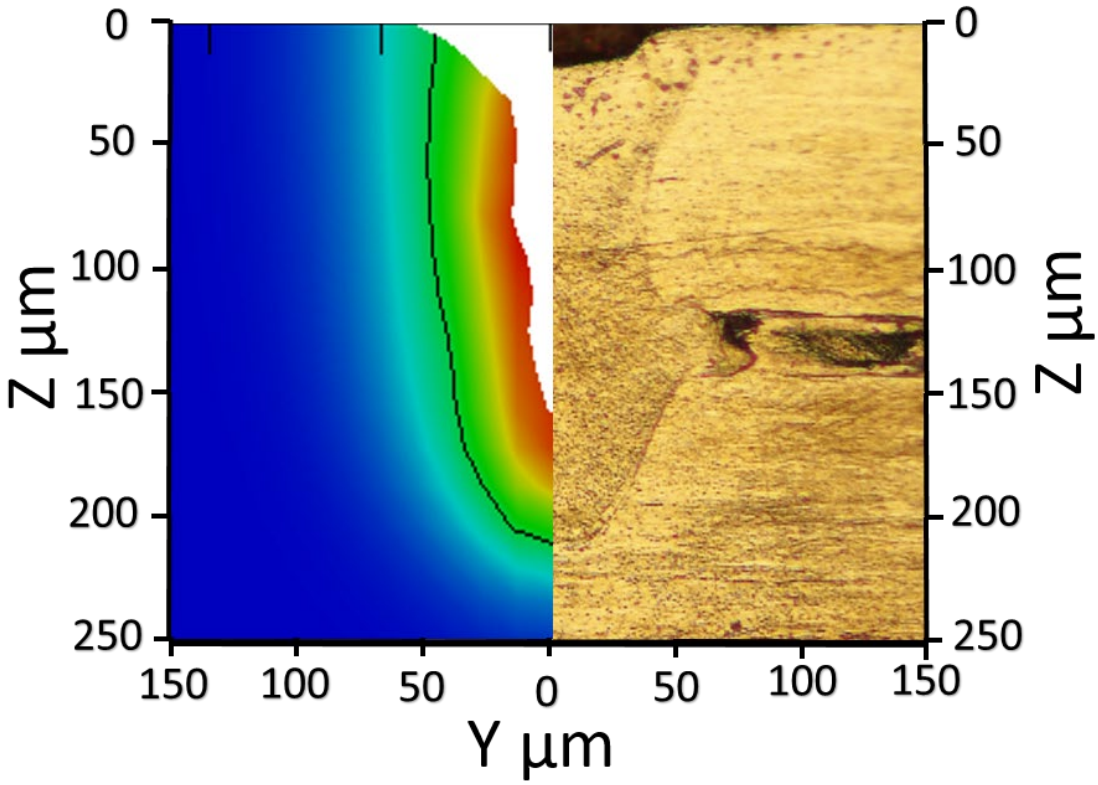

Fig. 4. Comparison of melt pool geometry in the cross-sectional view as estimated from numerically predicted solidus isotherm in the temperature map and experimentally measured weld macrograph at laser Process conditions: *P* = 100 W, time, *t* = 1.8 ms, laser beam spot radius, *r*0 = 25 µm and laser scanning speed 300 mm/s.

5. Conclusion

- Melt pool width and depth obtained from the developed numerical model depicts a good agreement with the experimentally measured data. The maximum deviation of width and depth is 16.2 % and 7.12 % respectively.
- The top view of welded sample at scanning speed 300 mm/s shows shining ripples, which visually conforms the good weld joint.
- The welded sample with scanning speed 300 mm/s provides the 54.53 % load to the base metal, which also conforms the good weld joint.
- The result shows the significant drop in hardness in melt pool (223±10 HV) as compare to interface (301±15) and base metal (415±10).
- The elongation of shear tensile test of welded lap joint shows very less elongation as compare with normal tensile test of base metal.

6. References

1. Jain, V.K., Dixit, U.S., Paul, C.P., Kumar, A., 2014. Micromanufacturing: a review—part II, Proceedings of the Institution of Mechanical Engineers, Part B: Journal of Engineering Manufacture 228, p. 995.
2. Meng, W., Yin, X., Fang, J., Guo, L., Ma, Q., Li, Z., 2019. Dynamic features of plasma plume and molten pool in laser lap welding based on image monitoring and processing techniques, *Optics & Laser Technology 109*, p. 168.
3. Zhou, S., Zhao, Y., Peng, Z., Ren, F., 2011. The investigation of laser Lap Welding process on high-strength galvanized steel sheets, *ISRN Mechanical Engineering*, Apr. *2011*.
4. Stanciu, E.M., Pascu, A., Roată, I.C., 2014. Lap joint laser welding of austenitic stainless steel thin sheets, *Advanced Materials Research* 1029, p. 134.
5. Ning, J., Hong, K.M., Inamke, G.V., Shin, Y.C., Zhang, L.J., 2019. Analysis of microstructure and mechanical strength of lap joints of TZM alloy welded by a fiber laser, *Journal of Manufacturing Processes 39*, p. 146.
6. Pellone, L., Inamke, G., Hong, K.M., Shin, Y.C., 2019. Effects of interface gap and shielding gas on the quality of alloy AA6061 fiber laser lap weldings, *Journal of Materials Processing Technology 268*, p. 201.
7. Cho, S.K., Yang, Y.S., Son, K.J., Kim, J.Y., 2004. Fatigue strength in laser welding of the lap joint, *Finite Elements in analysis and design 40*, p. 1059.
8. Miyazaki, Y., Furusako, S., 2007. Tensile shear strength of laser welded lap joints, *Nippon steel technical report 95*, p. 28.
9. Seang, C., David, A.K., Ragneau, E., 2013. Effect of Nd: YAG laser welding parameters on the hardness of lap joint: experimental and numerical approach.,*Physics Procedia 41*, p. 38.
10. Patel, S., Aggrawal, A., Kumar, A., Jain, V.K., 2018. High-Speed Conduction Mode Micro Laser Welding of Thin SS 304 Sheets: Modelling and Experimental Validation, 7th International and 28th All India Manufacturing Technology Design and Research Conference (AIMTDR), Dec. 2018.